Original Research

Diffusion-Weighted MR Study of Femoral Head Avascular Necrosis in Severe Acute Respiratory Syndrome Patients

Nan Hong, MD,[1]* Xiangke Du, MD,[1] Zhongshi Nie, MD,[2] and Sijun Li, MD[1]

Purpose: To evaluate the apparent diffusion coefficient (ADC) of femoral head avascular necrosis (AVN) in severe acute respiratory syndrome (SARS).

Materials and Methods: Seventy-nine SARS patients with hip pain underwent both conventional and diffusion-weighted MRI (b-value = 0–1000 seconds/mm^2). The abnormal regions on the diffusion-weighted images were outlined by using the conventional images as guides, and the ADCs were calculated. The ADC differences between normal and AVN femoral heads were compared.

Results: Of the 158 hips examined, 28 had AVN (11 with bilateral hip AVN, three with right hip AVN, and three with left hip AVN). The mean ADC was markedly greater in the AVN femoral head (1.66×10^{-3} mm^2/second $\pm$ 0.20) than in the normal femoral head (0.47×10^{-3} mm^2/second $\pm$ 0.082; $P < 0.0001$). There was no overlap between the normal and AVN femoral heads.

Conclusion: DWI can provide valuable information regarding the diffusion properties of femoral head AVN, and markedly increased diffusion was identified in AVN.

Key Words: hip, MR studies; hip, necrosis; magnetic resonance (MR); diffusion study; steroids
J. Magn. Reson. Imaging 2005;22:661–664.

FEMORAL HEAD AVASCULAR NECROSIS (AVN) was recently found in some patients suffering from severe acute respiratory syndrome (SARS) (1,2). The purpose of this study was to determine whether the apparent diffusion coefficient (ADC) of femoral head AVN differed from that of normal femoral head marrow. Most previous studies evaluated femoral head AVN using conventional T1-weighted images (T1WI), T2-weighted images (T2WI), and short-tau inversion recovery (STIR) sequences. Recently, diffusion-weighted MRI (DWI) has been used to study bone marrow (3–7). Because DWI reflects the random translational motion of the diffusion-driven water molecules within the tissue structure, we believed it could provide information about the differences between normal and pathologic tissues, and thus reveal the diffusion characteristics of femoral head AVN.

MATERIALS AND METHODS

Patients

The study group consisted of 79 SARS patients who fit the World Health Organization (WHO) case definition for SARS (8). The 79 patients included 60 women (age range = 21–63 years, mean age = 32.95 $\pm$ 8.69 years) and 19 men (age range = 21–52 years, mean age = 30.84 $\pm$ 7.82 years), with an overall age range of 21–63 years and mean age of 32.44 $\pm$ 8.49 years. None of the patients reported alcohol or intravenous drug abuse, and none had pre-SARS joint pain. Our institutional review board approved the study, and informed consent was obtained from each patient.

MRI Protocol

All 79 patients underwent MRI of the hips. The mean time for performing the MRI examination was 133 days after SARS or 131 days after steroid use. MRI was performed with a 1.5 T SIGNA CVi imager (GE Medical Systems, Milwaukee, WI, USA) equipped with a shielded magnetic field gradient of up to 40 mT/m. A body coil was used. All MRI examinations were performed using the following preset protocols: coronal T2-weighted fast spin-echo sequence (TR/TE = 3400/100 msec, 5-mm section thickness, 0.5-mm section gap, echo train length = 16, 256 $\times$ 224 matrix, 400-mm field of view (FOV), acquisition time = 1 minute 5 seconds); coronal STIR fat-suppressed sequence (TR/TE = 3420/100 msec, 5-mm section thickness, 0.5-mm section gap, echo train length = 16, 256 $\times$ 224 matrix, 400-mm FOV, acquisition time = 1 minute 6 seconds); coronal T1-weighted spin-echo sequence (TR/TE = 460/8.3 msec, 5-mm section thickness, 0.5-mm sec-

[1]Department of Radiology, Peking University People's Hospital, Beijing, China.
[2]Department of Radiology, General Hospital of Xishan Coal-Electricity Group, Taiyuan, China.
*Address reprint requests to: N.H., Department of Radiology, Peking University People's Hospital, 11 Xizhimen Nandajie, Xicheng District, Beijing, 100044, P. R. China. E-mail: hongnan@bjmu.edu.cn
Received 4 January 2005; Accepted 3 August 2005.
DOI 10.1002/jmri.20430
Published online 28 September 2005 in Wiley InterScience (www.interscience.wiley.com).

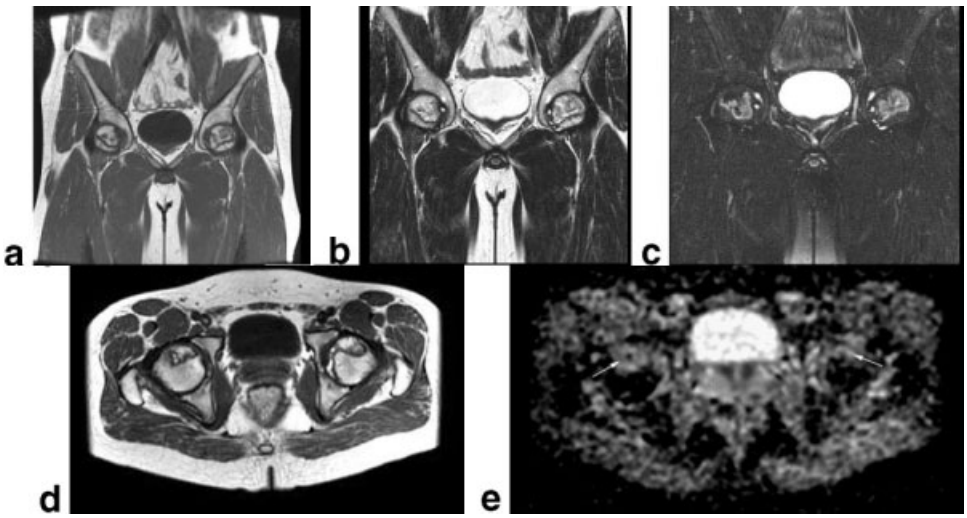

Figure 1. MR images of the hip of a 28-year-old man with SARS. Bilateral femoral head AVN was identified. Coronal T1WI (TR/TE = 460/8.3 msec) (**a**), coronal T2WI (3400/100) (**b**), coronal fat-suppressed STIR (TR/TE = 3420/100 msec) (**c**), and axial T1WI (TR/TE = 540/8.3 msec) (**d**) show AVN of the bilateral femoral head. **e:** Axial ADC map (TR/TE = 4000/76 msec, b = 0, and 1000 seconds/mm^2) shows a marked localized increase (arrow) in diffusion.

tion gap, 256 × 224 matrix, 400-mm FOV, acquisition time = 1 minute, 11 seconds), followed by an axial T1-weighted spin-echo sequence (TR/TE = 540/8.3 msec, 5-mm section thickness, 1.5-mm section gap, 256 × 224 matrix, 400-mm FOV, acquisition time = 2 minutes 4 seconds); and an axial diffusion-weighted echo-planar imaging (EPI) sequence (TR/TE = 4000/76 msec, 5-mm section thickness, 1.5-mm section gap, 128 × 128 matrix, 400-mm FOV, with a b-value of 1000 seconds/mm^2, number of excitations (NEX) = 2, acquisition time = 32 seconds), and bandwidth = 145 kHz. Diffusion gradients were applied along the three orthogonal (x, y, and z) directions, generating three images for each slice, together with an acquisition without diffusion weighting (b-value = 0).

MR Image Evaluation

The diagnosis of AVN was based on MRI criteria for AVN (9). Two experienced radiologists independently evaluated the conventional MR images and radiographs. The discordant cases were evaluated again in concert to reach a consensus diagnosis. The data were transferred to a PC workstation (Sun Microsystems, AW4.0_02) where the DWI data were postprocessed using Functool 2 (GE Medical Systems, Milwaukee, WI, USA). EPI distortion was corrected automatically. A user-defined ROI was placed in the center of the lesion, and the largest fitting circle or ellipse was positioned centrally. Since the margins of the lesions were irregular, ROIs could not be made with the same size and shape. The ROI selections were guided with the use of conventional T1WI, T2WI, and fat-suppressed STIR images, matching the coordinates of the lesions, and with the operator blinded to the ADC map signal. The same circle was then moved over the same area on the contralateral (normal) hip for measurement of the ADC. The average ADC is the mean diffusivity of three main diffusion directions (Dxx, Dyy, and Dzz), which indicates the overall evaluation of diffusion ability in each voxel. ADC was calculated using the following formula: ADC = (Dxx + Dyy + Dzz)/3, where Dxx, Dyy, and Dzz are the mean ADCs in the x, y, and z directions, respectively.

Statistics

A statistical analysis of the ADC was performed using Student's *t*-test. A *P*-value < 0.05 was considered significant.

RESULTS

AVN was identified in 28 of the 158 hips examined (17.72%, 11 patients with bilateral femoral head AVN, and six patients with ipsilateral femoral head AVN). All of the lesions were in class A according to the Mitchell classification system (10). A "double-line" sign (hyperintense inner border inside a hypointense margin) was seen in all hips on T2WI, and the margins of all the lesions were hyperintense on fat-suppressed STIR images. Increased signal intensity could be seen on ADC maps (Fig. 1). The mean ADC of the normal femoral head was 0.47×10^{-3} mm^2/second ± 0.082. In patients with AVN, the mean ADC was markedly increased, with a mean value of 1.66×10^{-3} mm^2/second ± 0.20. The difference between these two entities was statistically significant ($P < 0.0001$). There was no overlap between the normal and AVN femoral heads (Fig. 2).

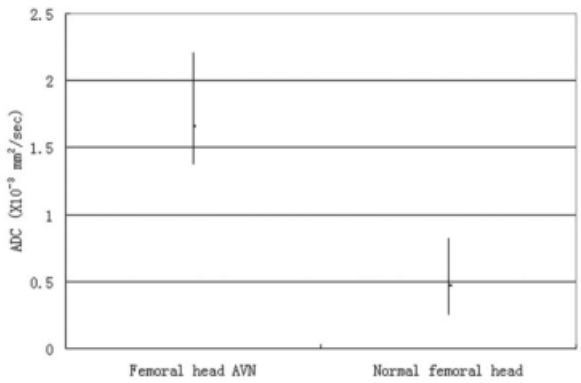

Figure 2. Graph showing the ADC values of femoral head AVN and normal femoral head.

DISCUSSION

The coronavirus has been found to be the primary cause of SARS (11–13). Recently, AVN was found in SARS patients (1,2). AVN represents a compromised circulation of blood to an area of bone. Existing hypotheses regarding its pathogenesis include vascular thrombosis, fat embolism, and vasculitis (9,14); however, the precise mechanism behind the development of AVN in SARS patients is still not clear. One study suggested that the use of steroids may be a factor (2). Another recent study reported that angiotensin-converting enzyme 2 is a functional receptor for the SARS coronavirus (15), which suggests that the coronavirus itself may lead to the development of AVN.

DWI is an MRI technique that allows the noninvasive examination of tissue structures at a molecular level (16). By applying equal and opposite gradients on either side of a refocusing lobe in a standard pulse sequence, diffusion sequences can identify subtle interstitial movement of water. In the absence of motion, tissue that is initially dephased becomes rephased by an applied equal and opposite gradient. In contrast, in the presence of motion, protons in tissue that is initially dephased do not become rephased by the equal and opposite gradient. The amount of recorded signal loss resulting from movement between the gradients is used as a marker of cellular diffusion or interstitial movement of water, and allows indirect evaluation of the tissue structure (17). The degree of signal attenuation due to diffusion in a voxel on a DWI sequence is logarithmically dependent on the ADC of that voxel and the b-value (18).

DWI was recently introduced for the evaluation of bone marrow (3–7). Some studies used DWI to evaluate vertebral compression fractures and showed that pathologic compression fractures were hyperintense, but that benign compression vertebral fractures were relatively hypointense (4). These studies suggest that hypercellularity by tumor cells reduced the extracellular space and mobility of water protons, leading to hyperintense diffusion-weighted images. Another study found that metastases could be either hypointense or hyperintense on DWI (3). Jaramillo et al (7) studied changes in diffusion with increasing duration of femoral head ischemia in piglets, and found that ADC decreased 26% after three hours of maximal abduction, and increased a mean of 27% after six hours and a mean of 75% after 96 hours after femoral neck ligature (7). The time-dependent changes in diffusion may reflect restriction of diffusion by cytotoxic edema, and tissue destruction leading to increased diffusion. A study by Nonomura et al (19) suggested a positive correlation between ADC value and bone marrow cellularity, with that fatty marrow having more restricted diffusion.

The normal femoral heads were hypointense on both the DWI and STIR images because the fat marrow signal was suppressed and the amount of free proton was negligible in the interstitial space, and thus the ADCs of the normal femoral head were low. One study revealed that the mean ADC values were 0.23×10^{-3} mm^2/second in normal vertebral bodies (18), which is a lower value than that in our study. In our study the mean ADC in the normal femoral head was 0.47×10^{-3} mm^2/second. The difference is probably due to the difference in hematopoietic states between the two studies.

Hematopoietic cells are sensitive to anoxia and usually die within 6–12 hours after the blood supply is removed. Osteocytes usually die within 12–48 hours, and marrow fat cells usually die within five days (20). Repair begins at the interface between necrotic and viable bone. Capillaries and undifferentiated mesenchymal cells grow into the dead marrow spaces, the macrophages degrade dead cellular and fat debris, and then mesenchymal cells differentiate into osteoblasts or fibroblasts (21). In our study the mean ADC in AVN was markedly increased compared to the normal femoral head (1.66×10^{-3} mm^2/second vs. 0.47×10^{-3} mm^2/second, $P < 0.0001$). In normal conditions, the trabeculae and fat cells may cause structural tortuosity, but when hematopoietic cells, osteocytes, and marrow fat cells die, the matrix components break down and the water diffusion in bone marrow becomes more active (20), leading to increased diffusion and an increased ADC. One study suggested that a smaller b-value increased the influence of perfusion but decreased the sensitivity to diffusion (22). When repair begins, capillaries grow into the dead marrow spaces. This perfusion effect could also be one of the reasons for the increased ADC values in our study, even though a high b-value (1000 seconds/mm^2) was used. Technical reasons may also account for differences in ADC values between various studies, such as an increased diffusion fraction and a decrease of perfusion contribution by sampling with multiple high b-value acquisitions, correction of bulk motion, T2 shine-through, etc.

There are several limitations to this study. First, we were unable to obtain histologic proof because no biopsy was performed. Second, limited spatial resolution, large magnetic susceptibility, and chemical shift artifacts may have resulted in severe geometric distortion and signal dropout (23). Third, because of the large magnetic susceptibility variations in the hip, the commercial EPI pulse sequence does not produce good diffusion-weighted images. However, since our results were focused mainly on the measurement of ADC values, the image quality was not vitally important to this study.

In conclusion, although conventional MRI is already a good tool for diagnosing AVN, the increased diffusion identified in AVN by DWI in this study suggests that DWI may be able to reveal the characteristics of femoral head AVN and thus provide additional information for such a diagnosis.

ACKNOWLEDGMENT

The authors gratefully acknowledge Tao Liu for preparing this manuscript, and Quansheng Jiang, MRI chief technologist, for assistance.

REFERENCES

1. Jiang XX, Wang XY, Xiao JX. MRI in the following up of the osteonecrosis in SARS patients. Chin J Med Jmaging Technol 2003;19: 1279–1280.

2. Hong N, Du XK. Avascular necrosis of bone in severe acute respiratory syndrome. Clin Radiol 2004;59:602–608.
3. Castillo M, Arbelaez A, Smith K, Fisher LL. Diffusion-weighted MR imaging offers no advantage over routine noncontrast MR imaging in the detection of vertebral metastases. AJNR AM J Neuroradiol 2000;21:948–953.
4. Bauer A, Stabler A, Bruning R, et al. Diffusion-weighted MR imaging of bone marrow: differentiation of benign versus pathologic compression fractures. Radiology 1998;207:349–356.
5. Ward R, Caruthers S, Yablon C, Blake M, DiMasi M, Eustace S. Analysis of diffusion changes in posttraumatic bone marrow using navigator-corrected diffusion gradients. AJR Am J Roentgenol 2000;174:731–734.
6. Yasumoto M, Nonomura Y, Haraguchi K, Ito S, Ohashi I, Shibuya H. MR detection of iliac bone marrow involvement by malignant lymphoma with various MR sequences including diffusion-weighted echo-planar imaging. Skeletal Radiol 2002;31:263–269.
7. Jaramillo D, Connolly SA, Vajapeyam S, et al. Normal and ischemic epiphysis of the femur: diffusion MR imaging—study in piglets. Radiology 2003;227:825–832.
8. World Health Organization. Case definitions for surveillance of severe acute respiratory syndrome (SARS). Available at http://www.who.int/csr/sars/casedefinition/en.
9. Tang S, Chan TM, Lui SL, Li FK, Lo WK, Lai KN. Risk factors for avascular bone necrosis after renal transplantation. Transplant Proc 2000; 32:1873–1875.
10. Mitchell DG, Rao VM, Dalinka MK, et al. Femoral head avascular necrosis: correlation of MR imaging, radiographic staging, radionuclide imaging, and clinical findings. Radiology 1987;162:709–715.
11. Ksiazek TG, Erdman D, Goldsmith CS, et al. A novel coronavirus associated with severe acute respiratory syndrome. N Engl J Med 2003;348:1953–1966.
12. Drosten C, Gunther S, Preiser W, et al. Identification of a novel coronavirus in patients with severe acute respiratory syndrome. N Engl J Med 2003;348:1967–1976.
13. Peiris JS, Lai ST, Poon LL, et al. Coronavirus as a possible cause of severe acute respiratory syndrome. Lancet 2003;361:1319–1325.
14. Imhof H, Breitenseher M, Trattnig S, et al. Imaging of avascular necrosis of bone. Eur Radiol 1997;7:180–186.
15. Li W, Moore MJ, Vasilieva N, et al. Angiotension-converting enzyme 2 is a functional receptor for the SARS coronavirus. Nature 2003; 426:450–454.
16. Le Bihan D, Breton E, Lallemand D, Grenier P, Cabanis E, Laval-Jeantet M. MR imaging of intravoxel incoherent motions: applications to diffusion and perfusion in neurologic disorders. Radiology 1986;161:401–407.
17. Ward R, Caruthers S, Yablon C, Blake M, DiMasi M, Eustace S. Analysis of diffusion changes in posttraumatic bone marrow using navigator-corrected diffusion gradients. AJR Am J Roentgenol 2000;174:731–734.
18. Chan JHM, Peh WCG, Tsui EYK, et al. Acute vertebral body compression fractures: discrimination between benign and malignant causes using apparent diffusion coefficients. Br J Radiol 2002;75: 207–214.
19. Nonomura Y, Yasumoto M, Yoshimura R, et al. Relationship between bone marrow cellularity and apparent diffusion coefficient. J Magn Reson Imaging 2001;13:757–760.
20. Burgener FA, Meyers SP, Tan RK, Zaunbauer W. Joint disease. In: Burgener FA, Meyers SP, Tan RK, Zaunbauer W. editors. Differential diagnosis in magnetic resonance imaging. New York: Thieme Stuttgart; 2002. p 360–362, 386–388.
21. Lee CK, Hansen MT, Weiss AB. The "silent hip" of idiopathic ischemic necrosis of the femoral head in adults. J Bone Joint Surg 1980;62A:795–800.
22. Le Bihan D. Molecular diffusion nuclear magnetic resonance imaging. Magn Reson Q 1991;7:1–30.
23. Le Bihan D. Differentiation of benign versus pathologic compression fractures with diffusion-weighted MR imaging: a closer step toward the "holy grail" of tissue characterization? Radiology 1998; 207:305–307.